Design of a single all-silicon ring resonator with a 150 nm FSR and a 100 nm tuning range around 1550 nm

Ang Li,[1,2,*] Qiangsheng Huang,[1,3] and Wim Bogaerts[1,2,4]

[1] *Photonics Research Group, Department of Information Technology, Ghent University-IMEC, Ghent, Belgium.*

[2] *Center for Nano- and Biophotonics (NB-photonics), Ghent University, Belgium.*

[3] *State Key Laboratory for Modern Optical Instrumentation, Centre for Optical and Electromagnetic Research, Zhejiang Provincial Key Laboratory for Sensing Technologies,Zhejiang University, Hangzhou, China.*

[4] *Luceda Photonics, Dendermonde, Belgium.*

compiled: November 4, 2015

We present a novel and simple method to obtain an ultra-wide free spectral range (FSR) silicon ring resonator together with a tuning range covering the entire spectrum from 1500 nm to 1600 nm. A ring resonator with a large FSR together with a high Q factor, high tuning efficiency, low fabrication cost and complexity is desired for many applications. In this paper, we introduce a novel way to make such a ring resonator, which takes advantage of the well known resonance-splitting phenomenon. It is a single ring resonator with a FSR more than 150 nm around 1550 nm and has an easy thermo-optic tunability which can produce a tuning range around 90 nm or even more. Moreover, the device is simple to implement and can be fabricated in standard CMOS technology without requiring any kind of complicated processing or extra materials. The potential applications include single mode laser cavities, WDM filters, (de)multiplexers, optical sensors and integrated reflectors.

OCIS codes: (230.5750) Resonators; (230.7408) Wavelength filtering devices; (230.3120) Integrated optics devices; (280.4788) Optical sensing and sensors; (140.3570) Lasers, single-mode.

http://dx.doi.org/10.1364/XX.99.099999

1. Introduction

Microring resonators (MRR) have proven to be one of the most intensively used components in various applications, covering laser cavities, WDM filters, optical sensors, optical (de)multiplexers, all optical signal processing and more [1–6]. Silicon photonics is a very attractive platform to implement MRRs because of its high index contrast and compatibility with CMOS technology [7, 8]. This allows the fabrication of compact rings with small roundtrip length, leading to a large *free spectral range* (FSR). Most applications desire a ring resonator with a large FSR, wide *tuning range*, low *insertion loss* (IL), high *quality Q* factor, narrow *bandwidth* (BW) as well as low fabrication cost and complexity. However, these performance indicators cannot all be optimized at the same time, there is always a trade-off. For instance, the most straightforward way to get a ring resonator with a large FSR is to shorten its length, as the FSR is inversely proportional to the roundtrip length: $FSR = \frac{\lambda_0^2}{n_g L}$, here λ_0 is the resonance wavelength, n_g and L are the group index and total length of the ring waveguide, respectively.

But it is not possible to reduce the roundtrip length of the ring indefinitely. First of all, this will complicate the tuning scheme. Moreover, a very short length means a very sharp bend radius, sometimes smaller than 5 μm in silicon strip waveguides. This can lead to significant bend loss as well as bend/straight transition loss [9, 10], and make the ring more vulnerable to sidewall roughness as the mode profile in the bend waveguide is positioned closer to the outer wall. It is also difficult to obtain the correct coupling coefficient in the coupling sections because of the extremely short coupling length. All these factors impose a lower limit on the ring roundtrip length, and therefore an upper limit on the FSR.

Most applications limit the operational wavelength range of the ring to a single FSR. In silicon nanophotonic waveguides, the widest practical FSRs are of the order of 40 nm in the telecommunication C-band around 1550 nm [11] and the tuning efficiency is fixed at a value around 370 nm/RIU (refractive index unit), according to equation (1)[8], where the $\Delta\lambda, \Delta n_{eff}$ is the resonance wavelength shift and the effective index change, respectively. This tuning efficiency generates a tuning range limited to 7 nm if thermo-optic effect is applied, as the temperature variation induced by heater is generally less

* Corresponding author: ang.li@ugent.be

than 100 K and the thermo-optic coefficient of Silicon is 1.8×10^{-4} K^{-1}[12]. A ring resonator that has a much wider FSR, or is even free of any FSR, and can be tuned in a much wider range by simple thermo-optic effect, while at the same time does not suffer from implementation or performance limitations is therefore highly desirable.

$$\frac{\Delta\lambda}{\Delta n_{eff}} = \frac{\lambda_0}{n_g} \tag{1}$$

There has been other work proposing different methods to implement ring resonators with a very wide FSR [11, 13–16]. Apart from drastically reducing the bend radius, these methods can be classified in two categories: the use of the Vernier effect in multiple rings [15, 16]; and the use of intra-ring reflectors which require complicated processing or CMOS incompatible materials[13, 14, 17].

Multiple rings will impose additional requirements to the design accuracy and fabrication tolerance, as the resonance wavelength and bandwidth of the individual rings need to be extremely well matched. If not the multi-ring configuration can result in a split resonance. Moreover, the tuning efficiency is relatively poor and the resonance mode is hard to move continuously in the spectrum, moreover the well known problem of backscattering induced splitting is not considered and cannot be compensated [18].

An alternative is to introduce reflectors into the ring to induce a strong coupling between the clockwise and the counterclockwise propagating mode. Bragg gratings can be used to this effect, but the need for high-resolution e-beam lithography negates some of the advantages of current silicon photonics technologies. The same can be said for the use of metal particles as a back-reflector, which would introduce material incompatibilities. Moreover, extra loss mechanisms are accompanied with Bragg grating or metal particles. As clearly shown in [13], the Q factor as well as the extinction ratio of the resonance is quite poor. Again, these methods, even though they make use of deliberate backreflection, cannot compensate for unintentional, stochastic backscattering along the circumference of the ring.

Our device presented in this paper is a simple structure consisting of a ring resonator with a loop-MZI reflector inside the ring to intentionally introduce reflection. The device is accompanied with an ultra-wide FSR that spans more than 150 nm. Besides, by implementing two phase shifters, which can be based on simple thermo-optic effect, its tuning range can almost cover the whole spectrum from 1500 nm to 1600 nm, this is equivalent to a tuning efficiency 13 times higher than that of a normal silicon ring resonator. Moreover, for most of the former literature, the ring can only be configured as an all-pass ring, thus the applications are limited. The device we propose could be configured as either an all pass or an add drop ring resonator.

The paper is constructed in the following way: in section 2 we will explain schematic of the device as well as the theory behind this phenomenon by means of *temporal Coupled Mode Theory* (tCMT). In the section 3 after that, the design principles, detailed characterisation and simulation results by using circuit simulator-Caphe [19] will be given. Finally we will conclude our work.

2. Theory and Schematic

In this section, we will first use temporal Coupled Mode Theory (tCMT) to explain how reflection inside the MRR could significantly influence the extinction ratio of MRR. Then we will introduce how to get an ultra wide FSR by taking advantage of this phenomenon. Finally we will give and briefly introduce the schematic for our device.

2.A. Extinction Ratio Modified by Reflection Inside the MRR

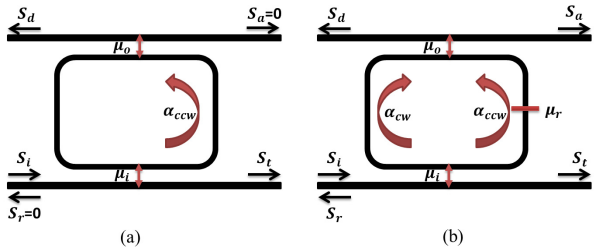

Fig. 1: Schematic of the tCMT model for ring resonators. (a) An ideal ring resonator has no reflection inside, thus only one circulating mode is activated by corresponding input port. (b) In a ring resonator with internal backreflection, the two modes are coupled thus simultaneously active.

tCMT has been used intensively to analyze a ring resonator with or without reflection [18, 20–22]. We will first use tCMT to build a model for an ideal MRR and then build a model for a MRR with reflection inside, to clearly and quantitatively show how the reflection will influence the performance (resonance wavelength, extinction ratio etc.) of the ring.

2.A.1. tCMT for Ideal MRR

For an ideal MRR without any kind of reflection or backscattering inside, there is only one circulating mode when only one port is injected with light as shown in Fig. 1 (a). According to tCMT, equations describing the circulating mode α_{ccw} as well as the transmitted field at through port S_t are given in equation (2) and (3) [20, 21]:

$$\frac{d\alpha_{ccw}}{dt} = j\omega_0\alpha_{ccw} - (\frac{1}{\tau_i} + \frac{1}{\tau_o} + \frac{1}{\tau_l})\alpha_{ccw} - j\mu_i S_i \tag{2}$$

$$S_t = S_i - j\mu_i\alpha_{ccw} \quad S_d = -j\mu_o\alpha_{ccw} \quad S_a = S_r = 0 \tag{3}$$

Here, α_{ccw} stands for the energy amplitude of the counterclockwise propagating mode, normalized such

that $|\alpha_{ccw}|^2$ represents the total energy of this mode. S_x refer to the wave amplitude at each port, quite similar to the electric filed amplitude, as $|S_x|^2$ also has the unit of power. The decay rates $\frac{1}{\tau_i}$ and $\frac{1}{\tau_o}$ describe the transfer of energy to the input and output bus waveguides, and $\frac{1}{\tau_l}$ represents the intrinsic ("unloaded") roundtrip loss. The coupling in the directional couplers μ_i and μ_o are related to these decay rates and the field coupling coefficients κ_i and κ_o as in equation (4)[21]:

$$\mu_i^2 = \kappa_i^2 \frac{c}{n_g L} = \frac{2}{\tau_i} \quad \mu_o^2 = \kappa_o^2 \frac{c}{n_g L} = \frac{2}{\tau_o} \quad \alpha_l^2 \frac{c}{n_g L} = \frac{2}{\tau_l} \tag{4}$$

Here, the c, n_g, L are light speed in vacuum, group index of the waveguide and physical length of the ring, respectively. The term α_l denotes the roundtrip loss of electric field in the MRR, and is similar in concept as the field coupling coefficients κ_i and κ_o. After solving the equations (2) and (3), we can extract a straightforward formula for the amplitude as well as the power at each port as in equation (5) and (6):

$$\frac{S_t}{S_i} = 1 - \frac{\frac{2}{\tau_i}}{j(\omega - \omega_0) + (\frac{1}{\tau_i} + \frac{1}{\tau_o} + \frac{1}{\tau_l})} \tag{5}$$

$$\frac{|S_t|^2}{|S_i|^2} = 1 - \frac{\frac{2}{\tau_i}(\frac{2}{\tau_o} + \frac{2}{\tau_l})}{(\omega - \omega_0)^2 + (\frac{1}{\tau_i} + \frac{1}{\tau_o} + \frac{1}{\tau_l})^2} \tag{6}$$

Clearly, the resonance is a Lorentzian-shape line. Its central frequency ω_0 or wavelength λ_0 is entirely determined by the physical length L and effective index n_{eff} of the MRR. The extinction ratio is directly related with the transmission at the resonance frequency $\omega = \omega_0$, which is shown in equation (7):

$$P_i = 1 - \frac{\frac{2}{\tau_i}(\frac{2}{\tau_o} + \frac{2}{\tau_l})}{(\frac{1}{\tau_i} + \frac{1}{\tau_o} + \frac{1}{\tau_l})^2} \tag{7}$$

When $\frac{1}{\tau_i} = \frac{1}{\tau_o} + \frac{1}{\tau_l}$, then $P_i = 0$, or physically speaking, when the power coupled into the MRR from the input port i equals the roundtrip loss plus the power coupled to the output port d, we get critical coupling, which gives us the largest extinction ratio. For an all-pass ring, where $\frac{1}{\tau_o} = 0$, the critical coupling condition is changed to $\kappa_i^2 = \alpha_l^2$. It is in good correspondence with former literature which describes critical coupling in the space domain [8]. In [8], the critical coupling condition for an all-pass MRR gives the same result, while for an add-drop MRR it is written as $(1 - \kappa_i^2) = (1 - \kappa_o^2)(1 - \alpha_l^2)$. After some transformation we get $\kappa_i^2 = \kappa_o^2 + \alpha_l^2 - \kappa_o^2 \alpha_l^2$, where the term $\kappa_o^2 \alpha_l^2$ is generally two orders of magnitudes smaller, and therefore negligible. at that point it becomes the same as our condition, which is $\kappa_i^2 = \kappa_o^2 + \alpha_l^2$.

2.A.2. tCMT model for a MRR with Reflection Inside

After having an understanding of the tCMT and the concept of critical coupling, we will derive the equations for MRR with internal reflection. The essential difference with an ideal MRR is that, due to reflection inside, the two degenerate circulating modes α_{cw} (clockwise), and α_{ccw} (counterclockwise) are coupled and activated simultaneously as illustrated in Fig. 1 (b). This leads to resonance splitting and a change in the extinction ratio. The equations for amplitudes of these modes are modified to equations (8) and (9):

$$\frac{d\alpha_{ccw}}{dt} = j\omega_0 \alpha_{ccw} - (\frac{1}{\tau_i} + \frac{1}{\tau_o} + \frac{1}{\tau_l})\alpha_{ccw} - j\mu_i S_i - j\mu_r \alpha_{cw} \tag{8}$$

$$\frac{d\alpha_{cw}}{dt} = j\omega_0 \alpha_{cw} - (\frac{1}{\tau_i} + \frac{1}{\tau_o} + \frac{1}{\tau_l})\alpha_{cw} - j\mu_r^* \alpha_{ccw} \tag{9}$$

There is an extra term of μ_r appearing in these equations. Here we consider a simple coupling of these two modes, which means the coupling is conservative instead of dissipative. Similar to μ_o and μ_i, μ_r refers to the mutual coupling between these two modes. But slightly different in its dependency on the field reflectivity r as given in equation (10):

$$\mu_r^2 = r^2 (\frac{c}{n_g L})^2 \tag{10}$$

The equation to get S_t and S_d remains the same as equation (3) (note, even though the equations are the same, $\alpha_{cw}, \alpha_{ccw}$ are modified), but S_a and S_r are modified to equation (11). And this time, we get quite a different formula for S_t as in equation (12):

$$S_a = -j\mu_o \alpha_{cw} \quad S_r = -j\mu_i \alpha_{cw} \tag{11}$$

$$\begin{aligned} \frac{S_t}{S_i} =& 1 - \frac{2}{\tau_i} \frac{j(\omega - \omega_0) + (\frac{1}{\tau_i} + \frac{1}{\tau_o} + \frac{1}{\tau_l})}{[j(\omega - \omega_0) + (\frac{1}{\tau_i} + \frac{1}{\tau_o} + \frac{1}{\tau_l})]^2 + |\mu_r|^2} \\ =& 1 - \frac{2}{\tau_i} (\frac{0.5}{j(\omega - \omega_1) + (\frac{1}{\tau_i} + \frac{1}{\tau_o} + \frac{1}{\tau_l})} \\ & + \frac{0.5}{j(\omega - \omega_2) + (\frac{1}{\tau_i} + \frac{1}{\tau_o} + \frac{1}{\tau_l})}) \end{aligned} \tag{12}$$

Clearly, instead of one single Lorentzian-shape resonance as in equation (5), there are now two Lorentzian-shape resonances with their own resonance frequency $\omega_1 = \omega_0 + |\mu_r|, \omega_2 = \omega_0 - |\mu_r|$. The modified power transmission P_r at the resonance frequency ω_1 or ω_2 are given in equation (13). Note that in equation (13), $\frac{1}{\tau_i}, \frac{1}{\tau_o}, \frac{1}{\tau_l}$ and μ_r are already replaced by equations (4) and (10).

$$\begin{aligned} P_r &= (\frac{\frac{2}{\tau_o} + \frac{2}{\tau_l}}{\frac{2}{\tau_i} + \frac{2}{\tau_o} + \frac{2}{\tau_l}})^2 + \frac{(\frac{2}{\tau_i})^2 - 2\frac{2}{\tau_i}(\frac{2}{\tau_o} + \frac{2}{\tau_l})}{(\frac{2}{\tau_i} + \frac{2}{\tau_o} + \frac{2}{\tau_l})^2 + 16|\mu_r|^2} \\ &= (\frac{\kappa_o^2 + \alpha_l^2}{\kappa_i^2 + \kappa_o^2 + \alpha_l^2})^2 + \frac{(\kappa_i^2)^2 - 2\kappa_i^2(\kappa_o^2 + \alpha_l^2)}{(\kappa_i^2 + \kappa_o^2 + \alpha_l^2)^2 + 16r^2} \end{aligned} \tag{13}$$

Note that, if $r = 0$, equation (13) becomes identical to equation (7). Because of the existence of reflection μ_r, the transmission at resonance becomes impossible to directly analyze in a quantitative way. By assuming the MRR is still at the original critical coupling point as an ideal MRR, we will see how the extinction ratio changes dramatically with the reflection. By making $\kappa_i^2 = \kappa_o^2 + \alpha_l^2$, P_r is modified to equation (14):

$$P_r|_{cp} = \frac{1}{4} - \frac{|\kappa|^4}{4|\kappa|^4 + 16r^2} \tag{14}$$

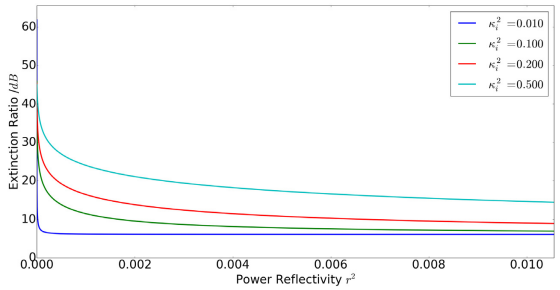

Fig. 2: At the critical coupling point, the extinction ratio drops dramatically with increasing reflection until it reaches an almost constant value. This phenomenon is one of the basic principles to obtain an ultra wide FSR ring resonator.

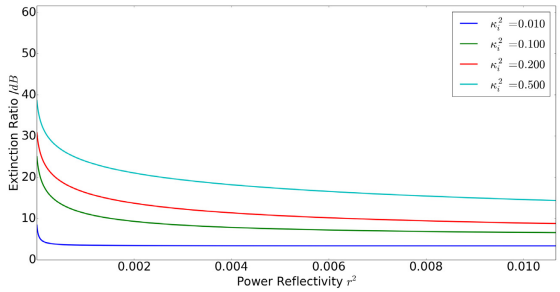

Fig. 3: This figure shows how the extinction ratio changes with reflectivity when the MRR deviates from its critical coupling point, and it's configured as $\kappa_i = \kappa_o$, which is the general case and easy to guarantee. Note that, the side mode suppression could be improved by simply increasing coupling coefficient.

In Fig. 2, we get the extinction ratio of a critically coupled MRR as a function of field reflectivity $|r|$ under different field coupling coefficient $|\kappa_i|$. Clearly, the extinction ratio drops dramatically with increasing reflectivity. This phenomenon is one of the basic principles in our paper to get an ultra wide FSR in a MRR. We will introduce a reflector whose reflection spectrum is strongly wavelength dependent. In a specific configuration, we can obtain a spectrum where only a single resonance suffers zero reflection while the others within a wavelength range of 150 nm suffer from a strong reflection.

Before this, we investigate how the extinction ratio changes with reflectivity when the MRR is not critically coupled. This is important because in reality, it's very difficult to fabricate a ring where all coupling factors and losses are matched at the correct wavelength, due to fabrication variability. So exploring the behavior of the ring in the non-critical-coupling regime can also be considered as a fabrication tolerance analysis of the device. In Fig. 3 the dependency of extinction ratio on reflectivity $|r|$ under different coupling strength is given. In contrast to Fig. 2, the MRR is not configured at the critical coupling point. The loss factor α_l^2 is set to be constant at 0.0114 corresponding with a 0.05 dB roundtrip power loss and κ_i is set to be identical with κ_o, which is often the case and easier to ensure than an absolute coupling coefficient.

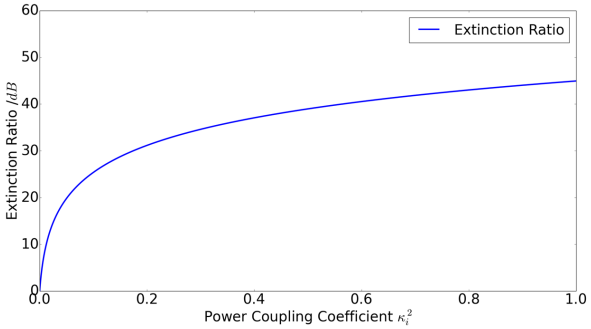

(a) Extinction ratio as a function of coupling coefficient.

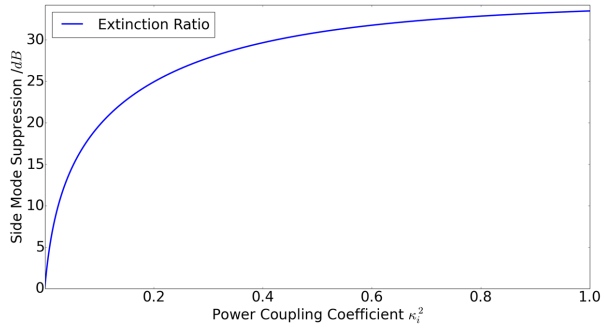

(b) Side Mode Expression as a function of coupling coefficient.

Fig. 4: These figures show how the extinction ratio as well as the side mode suppression changes with power coupling coefficient when the MRR is away from its critical coupling point, and designed as $\kappa_i = \kappa_o$.

It's natural to expect a performance degradation due to the deviation from the critical coupling condition, which appears in the smaller side mode suppression and the smoother slope. However, the extinction ratio still drops significantly with increasing reflectivity, and it's noteworthy that the extinction ratio of the remaining resonance as well as the side mode suppression can be

improved by simply increasing the coupling coefficient, as illustrated in Fig. 4. This device is then quite practical, as we require no exact configuration such as critical coupling. Another advantage is that in this configuration the MRR becomes less sensitive to stochastic backscattering, which we will discuss in detail in later section.

2.B. Ultra Wide FSR MRR

Now we get to know that the reflection will significantly reduce the extinction ratio of the resonance. If we could find a way to make all but one resonance of the ideal MRR suffer from strong reflection while the rest one suffers zero reflection, then only one resonance has a large extinction ratio while all the rest have very small extinction ratio, and we could consider this MRR as FSR free. This requirement could be achieved by introducing a tunable reflector consisting of a loop Mach-Zehnder interferometer (MZI), as shown in Fig. 5. This circuit can generate various reflection spectra based on the lengths L_1, L_2 of its two arms. Section 3 discusses the design and simulation in detail.

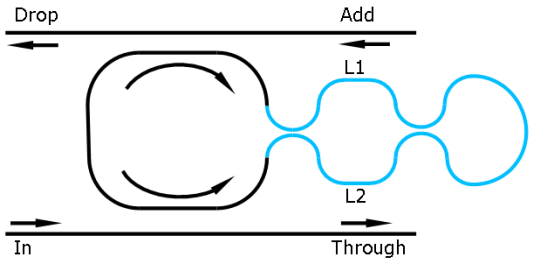

Fig. 5: The ring resonator has a loop MZI tunable reflector inside, which introduces a wavelength-dependent intentional reflection that couples two circulating modes. Strong reflection will lead to visible peak splitting, and it will in turn influence the extinction ratio of the resonance. By properly designing the arm lengths of the MZI, we can obtain a spectrum where only one wavelength has zero reflection while the rest suffer strong reflection.

2.C. Schematic

The schematic of the MRR with an ultra wide FSR is given in Fig. 5. It consists of an MRR with an embedded asymmetric MZI reflector. This intentionally introduces a wavelength-dependent reflection which couples the two circulating modes (CW and CCW).

3. Design, Simulation and Analysis

3.A. Design

The key design parameter in the loop-MZI reflector is the length difference $\Delta L = L_1 - L_2$ between the two arms. The absolute length of each arm depends on the specific applications, for instance, for sensing we prefer a longer arm to capture more particles, however for filters

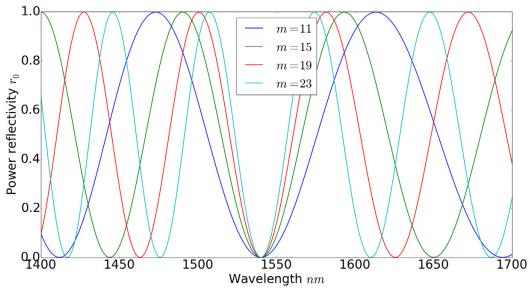

(a) The directional coupler performance is wavelength independent.

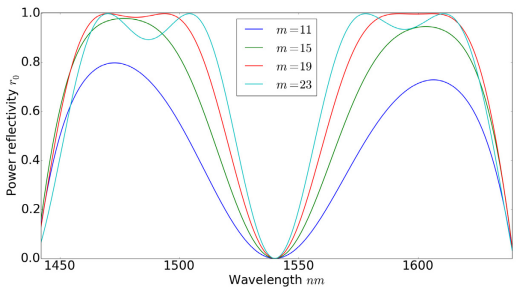

(b) A linear model for directional coupler extracted from FDTD simulation is added.

Fig. 6: Curves of the reflection spectra of the reflector. The directional couplers are designed to be 50/50 splitter.

or laser cavities, we could rather make them as short as possible to reduce the loss, foot print and the stochastic backscattering. The zero-reflection wavelength depends on the ΔL as in equation (15):

$$\frac{2\pi\Delta L n_{eff}}{\lambda} = m\pi \tag{15}$$

Here, m is the interference order, similar to a normal MZI. The simulated reflection spectra with various ΔL generated by the circuit simulator Caphe[19] is given in Fig. 6.

In the simplified case where the directional coupler is treated as an ideal, wavelength independent component, a larger ΔL will lead to a smaller FSR and a sharper slope. More interesting is the case where a realistic behavior of the directional coupler is used, with a linear wavelength dependency model extracted from an FDTD simulation. In that case the FSR seems to be independent of the ΔL, while the slope still shows the same trends with ΔL. This facilitates our design as we can now get a large FSR together with a sharp reflection slope.

3.B. Simulation

In Fig. 7, the simulated through port spectrum of our device is plotted. Here, $L_2 = 10\ \mu m$, $m = 23$, thus

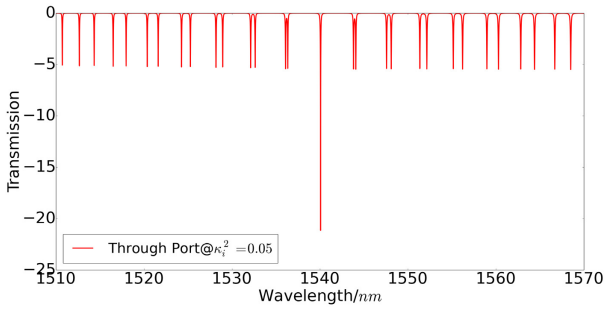

(a) $\kappa_i^2 = 0.05$

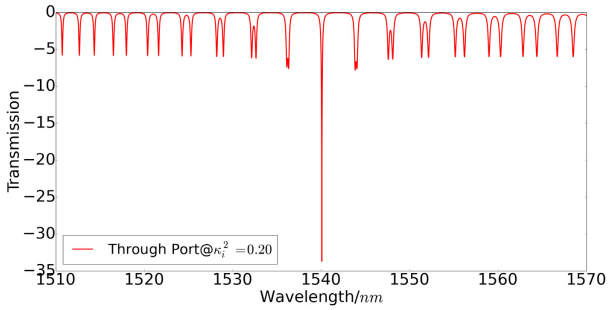

(b) $\kappa_i^2 = 0.2$

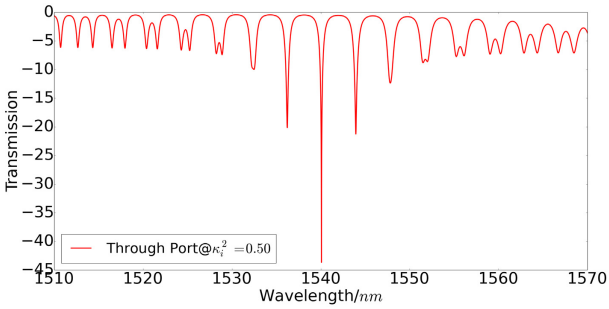

(c) $\kappa_i^2 = 0.5$

Fig. 7: A simulated through port of our device. The order m is chosen to be 23, and the MRR is set at the normal coupling condition $\kappa_i^2 = \kappa_o^2$.

$\Delta L = 7.44\ \mu m$, and the total roundtrip length is set to be around 150 μm and a resonance appears at 1540 nm. The roundtrip loss is set to be 0.05 dB (corresponding with a loss coefficient of 330 dB/m), and $\kappa_i = \kappa_o$. Corresponding with the theory, only the wavelength of zero reflection shows a large extinction ratio of the ring resonance, while the other resonances have a very small extinction ratio and a strong resonance splitting. Besides, we notice that, another part of the theory is also verified, which is, the side mode suppression and extinction ratio of the survived resonance could be increased by simply coupling more power into the ring, as also shown in Fig.7. Even though for large coupling coefficient, for instance, $\kappa_i^2 = 0.5$, the adjacent resonance modes start to arise, we can again suppress it by increasing the interference number m as this will sharpen the slope of the reflector spectrum. This feature will be also mentioned and illustrated in Fig. 13 in section 3.D.

3.C. Tunability

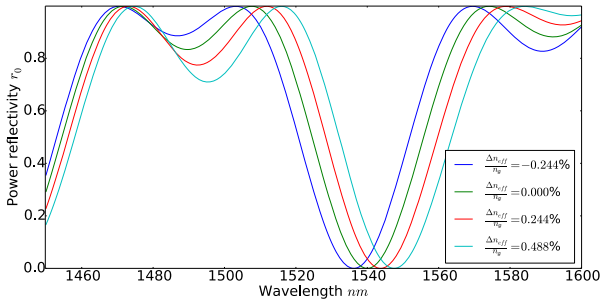

(a) The shift of the zero-reflection wavelength of the MZI based reflector induced by effective index n_{eff} change.

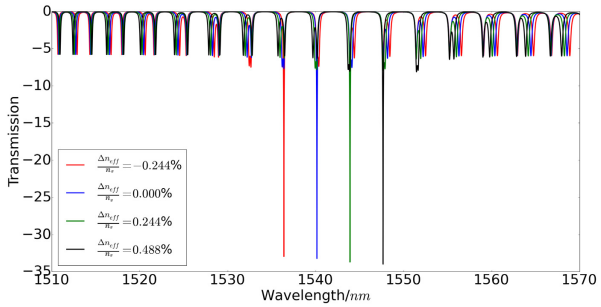

(b) The shift of the resonance wavelength of the MRR induced by effective index n_{eff} change.

Fig. 8: The whole device sees a same index change simultaneously, no matter whether this is induced by tuning or environment index change. Index changes cause a shift of the zero-reflection wavelength of the reflector and the resonance wavelength of the MRR at the same rate, and thus the MRR remains single mode. The tuning efficiency is the same as that of a normal silicon ring resonator.

We also look into the tunability of the device. As our device consists of two components that can be individually tuned, i.e. a ring resonator and a MZI based reflector, we can easily implement two very different tuning mechanisms or configurations by either tuning the whole device as discussed in section 3.C.1 or separate tuning of the ring and the reflector, as in section 3.C.2.

3.C.1. Common tuning

When the effective index of the waveguide changes on a global scale (e.g. by ambient temperature variations or background index change), both the zero-reflection wavelength as well as the resonance wavelength of the ring will drift at the same rate, as in equation (16). In Fig. 8, the spectra of both tunable reflector and MRR at different global effective indices are given.

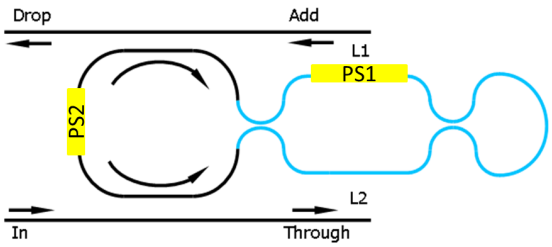

Fig. 9: Instead of using one common phase shifter for the whole device, we can implement two separate phase shifters to achieve individual tuning of the zero-reflection wavelength of the reflector and the resonance wavelength of the ring resonator. This configuration gives a much wider tuning range, within which the single mode can shift continuously.

$$\frac{\Delta\lambda}{\lambda_0} = \frac{\Delta n_{eff}}{n_g} \tag{16}$$

This configuration gives the same tuning efficiency and thus the same tuning range as a regular silicon ring resonator, which is not particularly efficient or wide. However, if we direct our attention from tuning to sensing application, this configuration could be quite promising, as no matter how large the background index changes, the single mode condition remains within the ultra-wide FSR and the resonance shifts corresponds with the background index change. In other words, this configuration could be very suitable for sensing applications, especially in large and rapid index change environment.

3.C.2. Separate Tuning

Alternatively, we can tune the ring and the reflector separately. In Fig. 9 we add two phase shifters for one arm of the reflector and the ring waveguide, respectively. Logically speaking, the phase shifter 1 (PS1) performs the function of resonance selection. It selects one out all of the resonances of the ring resonator to be the single mode of the device. The phase shifter 2 (PS2) takes the responsibility of comb tuning. It shifts the resonance spectrum of the ring resonator so that the single resonance selected by PS1 can be adjusted locally to cover a continuum rather than some discrete points. Mathematically speaking, the shift of the zero-reflection wavelength of the reflector is given in equation (17) and the shift of resonance mode of the ring resonator is given in equation (18).

$$\frac{\Delta\lambda_{ref}}{\lambda_0} = \frac{\Delta n_{ps1}}{n_g}\frac{L_{ps1}}{\Delta L} \tag{17}$$

$$\frac{\Delta\lambda_{ring}}{\lambda_0} = \frac{\Delta n_{ps1}L_{ps1} + \Delta n_{ps2}L_{ps2}}{n_g(L_{ps1}+L_{ps2}) + n_{eff}L_{rest}} \tag{18}$$

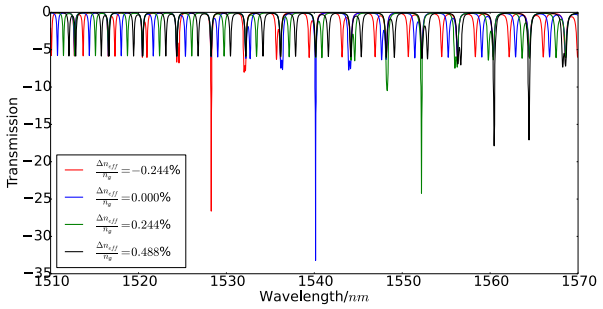

(a) Without PS2, the single mode resonance can only take place at some discrete wavelength points, as the zero-reflection wavelength of the reflector might not match the resonance of the ring resonator.

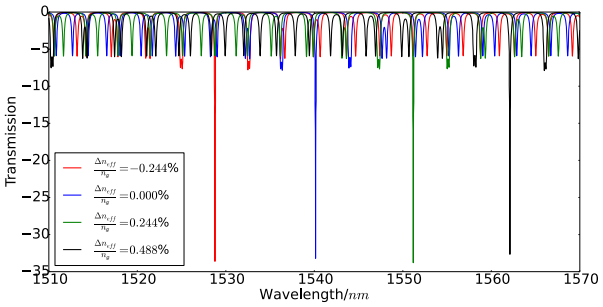

(b) With PS2 working, the single mode resonance can be tuned to more wavelength points, as the resonance of the ring resonator can now be aligned to the zero-reflection wavelength of the reflector.

Fig. 10: Two phase shifters are implemented, PS1 is responsible for the mode selection, while PS2 is in charge of comb tuning. Compared to common tuning configuration, with the same index change, we achieve a 4 times larger wavelength shift.

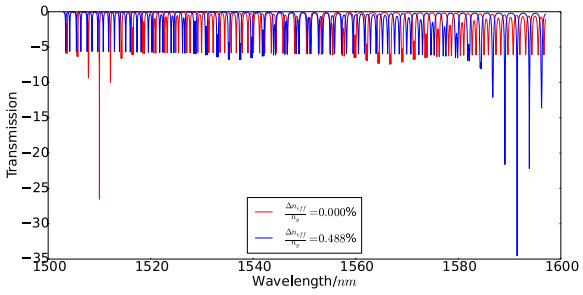

Fig. 11: When optimizing for a larger tuning range (at the cost of side-mode suppression ratio) we achieve a tuning rang almost as wide as 100 nm with the same index change.

- λ_0 is the wavelength of the single resonance. At original state, this is the zero-reflection wavelength of the reflector and it matches one of the resonance wavelength of the ring resonator.
- Δn_{ps1} and Δn_{ps2} are the effective index change

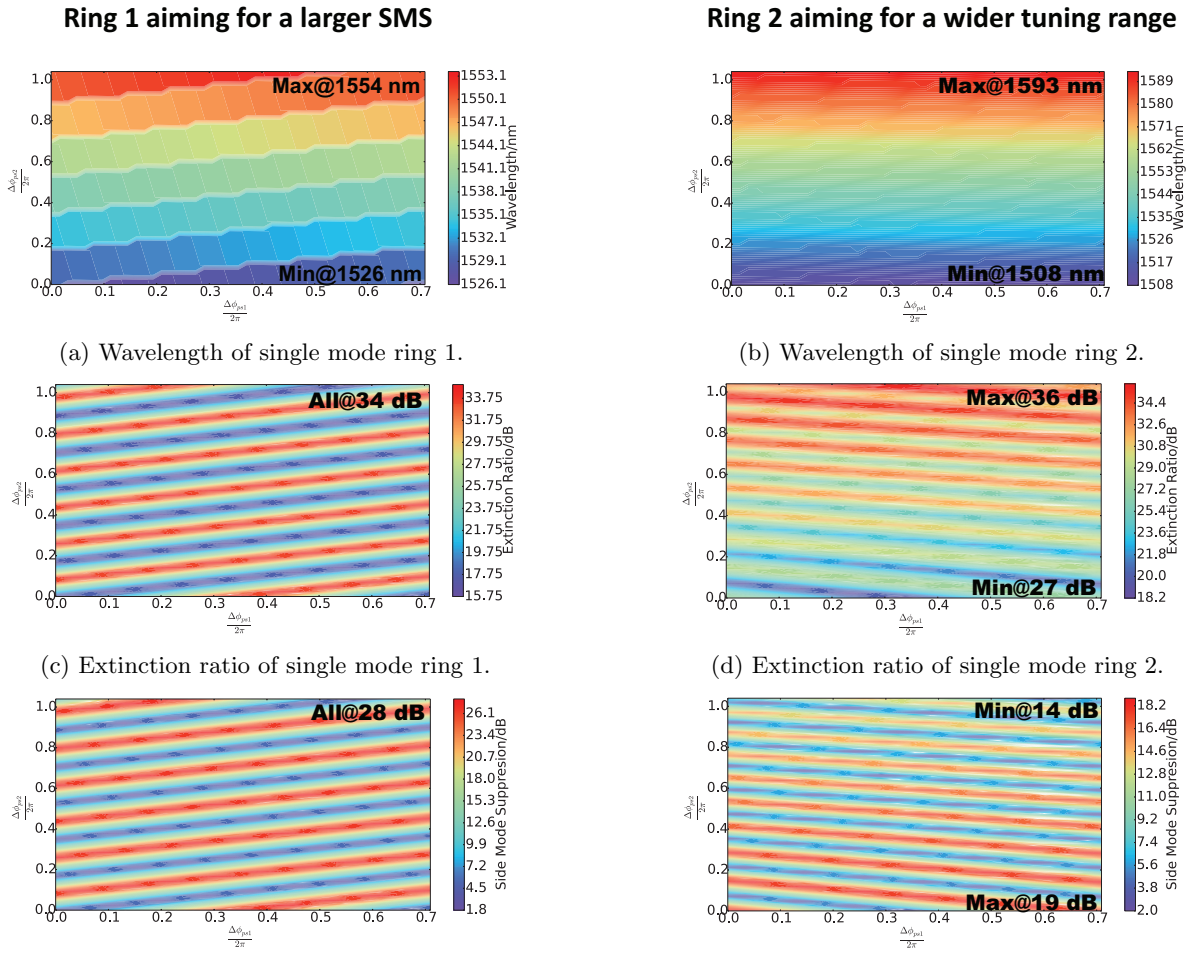

(a) Wavelength of single mode ring 1.

(b) Wavelength of single mode ring 2.

(c) Extinction ratio of single mode ring 1.

(d) Extinction ratio of single mode ring 2.

(e) Side mode suppression of single mode ring 1.

(f) Side mode suppression of single mode ring 2.

Fig. 12: Tuning map for the two phase shifters PS1 and PS2 ($\frac{\Delta\phi_{ps1}}{2\pi}$, $\frac{\Delta\phi_{ps2}}{2\pi}$) to achieve a continuous shift of the single mode resonance. Figures 12a, 12c and 12e give the results of the first design, where the parameters are designed in such a way that the SMSR of each wavelength is larger than 28 dB while the tuning range is only 30 nm, 4 times wider than that of a normal silicon ring resonator; The results of the modified design are illustrated in figures 12b, 12d and 12f, where the design parameters are changed to achieve a much wider tuning range around 90 nm at the price of a smaller SMSR, but still, at each wavelength, a SMSR larger than 14 dB can be guaranteed. Note that, 85 nm tuning range comes with a $\Delta\phi_{ps1}$ that is less than $0.7 \times 2\pi$, an even wide range is feasible by increasing $\Delta\phi_{ps1}$.

in PS1 and PS2 respectively. Similarly, L_{ps1}, L_{ps2} refer to the length of these two phase shifters.

- L_{rest} stands for the rest length of the ring resonator. $L_{rest} + L_{ps1} + L_{ps2}$ equals the total length of ring L.
- $\Delta\lambda_{ref}$ and $\Delta\lambda_{ring}$ are the shift of the zero-reflection wavelength of the reflector and the resonance wavelength of the ring resonator, respectively.

In contrast to the common tuning configuration, where the zero-reflection wavelength of the reflector and the resonance wavelength of the ring resonator shift at the same rate as in equation (16), they now shift at a very different rate. And the former one shifts much faster, depending on the value of L_{ps1} and ΔL. This provides the possibility to achieve a much wider tuning range. Specifically speaking, when $\Delta\lambda_{ref} = \Delta\lambda_{ring} + n\text{FSR}$, the new zero-reflection wavelength will again match one of the resonances of the ring resonator, thus the single mode condition remains. In the first design (where $L_2 = L_{ps2} = 10\ \mu m$, $m = 23$, L=150 μm), we achieve a $4\times$ higher tuning efficiency as illustrated in Fig. 10. In other words, with the same amount of effective index change (around 0.02), a tuning range of 30 nm is achieved instead of 7 nm. With further optimization ($L_2 = L_{ps2} = 50\ \mu m$, m=27, L=260 μm, and the same loss coefficient of 330 dB/m), the tuning range can expand to almost 100 nm, covering the spectrum from 1500 nm to 1600 nm, as illustrated in Fig. 11.

In Fig. 12, we give a more straightforward way to illustrate how to tune the PS1 and PS2 in order to achieve a continuous tuning of the single mode wavelength. Clearly, by tuning the index change of PS1 and PS2 in a feasible range (0-0.02), we can address a continuous shift of the single mode wavelength in a 30 nm span or a 90 nm span, depending on the design parameters of the MZI reflector. And at each wavelength, an extinction ratio larger than 30 dB and a side mode suppression larger than 26 dB (14 dB for 90 nm tuning span) can be guaranteed. In other words, a wide tuning range comes at the price of a smaller side mode suppression. However, the extinction ratio would be roughly independent of the length of PS1. Thus, the choice between a larger tuning range and a larger side mode suppression would depend on its specific application. These figures actually reveal another important feature of our device, which is the tolerance to the design accuracy. In other words, it does not require a ridiculously precise design of the individual optical length, as the single mode condition can be always achieved by dynamic tuning PS1 and PS2.

3.D. Effect of Unintentional Backscattering

Now we need to focus on some more practical issues, for instance, the well known backscattering in a SOI MRR. Backscattering can introduce 6-8 m^{-1} power reflectivity R_{bs} in a single-mode silicon strip waveguide with a dimension around 450 nm $\times$ 220 nm[23]. As mentioned above, the total length of our MRR is very flexible, and can be as short as 150 μm. The only drawback of the long length is its higher power reflection caused by the backscattering as it linearly scales with length.

In Fig. 13, we show the influence of backscattering for an MRR configured at normal coupling condition ($\kappa_i = \kappa_o$). As expected, the backscattering induced reflection will degrade the performance. When the length grows from 150 μm to 300 μm, and the power reflectivity caused by backscattering increases from 0.00105 to 0.0021, the single mode condition is damaged when the ring is configured at $\kappa_i^2 = 0.2$ and $m = 23$. But still, one could increase the performance by simply coupling more light and increasing the resonant number m, as illustrated in Fig. 13b and Fig. 13c.

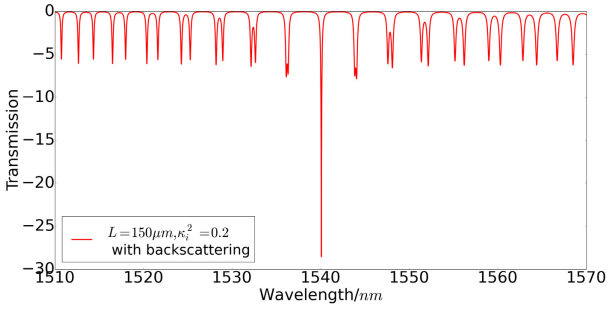

(a) $L = 150\ \mu m$, $\kappa_i^2 = 0.2$, $R_{bs} = 7 \times L$.

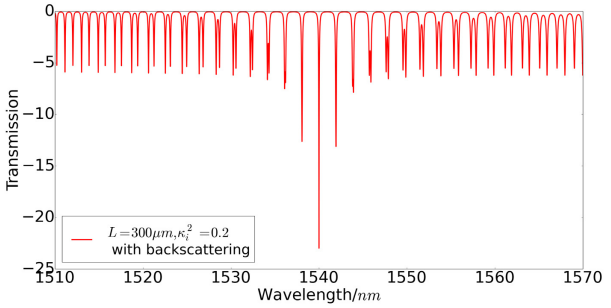

(b) $L = 300\ \mu m$, $\kappa_i^2 = 0.2$, $R_{bs} = 7 \times L$.

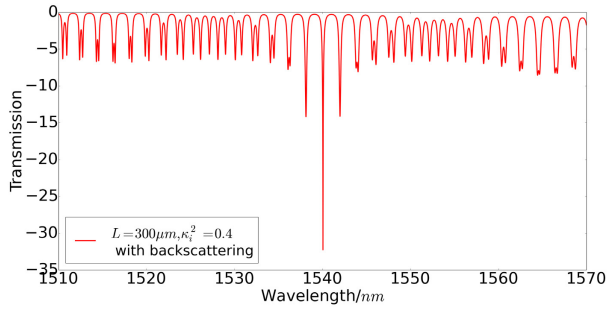

(c) $L = 300\ \mu m$, $\kappa_i^2 = 0.4$, $R_{bs} = 7 \times L$ and $m = 55$.

Fig. 13: Effect of unintentional backscattering on the performance of the MRR. When the length increases from 150 μm to 300 μm, and the corresponding power reflectivity of backscattering grows to $7L = 0.0021$, the side mode suppression shows a significant decrease. But we could increase the κ_i and the resonant number m to compensate as in Fig. 13c.

4. Conclusion

In conclusion, in this paper, we proposed a novel and simple method to obtain an all-silicon ring resonator which has only a single resonance in wavelength range of over 150 nm and a 13 times higher tuning efficiency compared to normal silicon ring resonator, that is to say, a tuning range almost as wide as 100 nm. One significant advantage is its simple structure, which is compatible with most of today's CMOS-based silicon photonics technology platforms. We provide a comprehensive and systematic theoretical model based on temporal coupled mode theory. Simulations with respect to the main design parameters are discussed, as well as the tolerance to the well known and unavoidable backscattering.

References

[1] M. A. Popovíc, T. Barwicz, M. R. Watts, P. T. Rakich, L. Socci, E. P. Ippen, F. X. Kärtner, and H. I. Smith, "Multistage high-order microring-resonator add-drop filters," Optics letters **31**, 2571–2573 (2006).

[2] J. H. Lee, I. Shubin, J. Yao, J. Bickford, Y. Luo, S. Lin, S. S. Djordjevic, H. D. Thacker, J. E. Cunningham, K. Raj *et al.*, "High power and widely tunable si hybrid external-cavity laser for power efficient si photonics wdm links," Optics express **22**, 7678–7685 (2014).

[3] B. E. Little, S. T. Chu, H. A. Haus, J. Foresi, and J.-P. Laine, "Microring resonator channel dropping filters," Lightwave Technology, Journal of **15**, 998–1005 (1997).

[4] J.-W. Hoste, S. Werquin, T. Claes, and P. Bienstman, "Conformational analysis of proteins with a dual polarisation silicon microring," Optics express **22**, 2807–2820 (2014).

[5] Q. Xu and M. Lipson, "All-optical logic based on silicon micro-ring resonators," Optics express **15**, 924–929 (2007).

[6] A. Malacarne, F. Gambini, S. Faralli, J. Klamkin, and L. Poti, "High-speed silicon electro-optic microring modulator for optical interconnects," Photonics Technology Letters, IEEE **26**, 1042–1044 (2014).

[7] W. Bogaerts, P. Dumon, D. Van Thourhout, D. Taillaert, P. Jaenen, J. Wouters, S. Beckx, V. Wiaux, and R. G. Baets, "Compact wavelength-selective functions in silicon-on-insulator photonic wires," Selected Topics in Quantum Electronics, IEEE Journal of **12**, 1394–1401 (2006).

[8] W. Bogaerts, P. De Heyn, T. Van Vaerenbergh, K. De Vos, S. Kumar Selvaraja, T. Claes, P. Dumon, P. Bienstman, D. Van Thourhout, and R. Baets, "Silicon microring resonators," Laser & Photonics Reviews **6**, 47–73 (2012).

[9] S. K. Selvaraja, W. Bogaerts, and D. Van Thourhout, "Loss reduction in silicon nanophotonic waveguide micro-bends through etch profile improvement," Optics Communications **284**, 2141–2144 (2011).

[10] H. Shen, L. Fan, J. Wang, J. C. Wirth, and M. Qi, "A taper to reduce the straight-to-bend transition loss in compact silicon waveguides," Photonics Technology Letters, IEEE **22**, 1174–1176 (2010).

[11] M. S. Nawrocka, T. Liu, X. Wang, and R. R. Panepucci, "Tunable silicon microring resonator with wide free spectral range," Applied physics letters **89**, 71110–71110 (2006).

[12] S. J. Emelett and R. Soref, "Design and simulation of silicon microring optical routing switches," Journal of lightwave technology **23**, 1800 (2005).

[13] D. Urbonas, A. Balčytis, M. Gabalis, K. Vaškevičius, G. Naujokaitė, S. Juodkazis, and R. Petruškevičius, "Ultra-wide free spectral range, enhanced sensitivity, and removed mode splitting soi optical ring resonator with dispersive metal nanodisks," Opt. Lett. **40**, 2977–2980 (2015).

[14] Q. Huang, K. Ma, and S. He, "Experimental demonstration of single mode- splitting in microring with bragg gratings," Photonics Technology Letters, IEEE **27**, 1402–1405 (2015).

[15] K. Oda, N. Takato, and H. Toba, "A wide-fsr waveguide double-ring resonator for optical fdm transmission systems," Lightwave Technology, Journal of **9**, 728–736 (1991).

[16] D. Geuzebroek, E. Klein, H. Kelderman, F. Tan, D. Klunder, and A. Driessen, "Thermally tuneable, wide fsr switch based on micro-ring resonators," (2002).

[17] R. Boeck, M. Caverley, L. Chrostowski, and N. A. F. Jaeger, "Grating-assisted silicon-on-insulator racetrack resonator reflector," Opt. Express **23**, 25509–25522 (2015).

[18] A. Li, T. V. Vaerenbergh, peter de heyn, Y. Xing, P. Bienstman, and W. Bogaerts, "Experimentally demonstrate the origin for asymmetric resonance splitting and contributions from couplers to backscattering in soi microrings," in "Advanced Photonics 2015," (Optical Society of America, 2015), p. IM2B.6.

[19] M. Fiers, T. V. Vaerenbergh, K. Caluwaerts, D. V. Ginste, B. Schrauwen, J. Dambre, and P. Bienstman, "Time-domain and frequency-domain modeling of nonlinear optical components at the circuit-level using a node-based approach," J. Opt. Soc. Am. B **29**, 896–900 (2012).

[20] M. A. Popović, "Theory and Design of High-Index-Contrast Microphotonic Circuits," Ph.D. thesis (2008).

[21] B. Little, S. Chu, H. Haus, J. Foresi, and J.-P. Laine, "Microring resonator channel dropping filters," Journal of Lightwave Technology **15**, 998–1005 (1997).

[22] H. Haus, *Waves and fields in optoelectronics*, Prentice-Hall Series in Solid State Physical Electronics (Prentice Hall, Incorporated, 1984).

[23] F. Morichetti, A. Canciamilla, and A. Melloni, "Statistics of backscattering in optical waveguides." Optics letters **35**, 1777–1779 (2010).